Draft version September 21, 2016
Preprint typeset using LaTeX style emulateapj v. 5/2/11

arXiv:1609.05850v2 [astro-ph.SR] 20 Sep 2016

PHOTOMETRIC MONITORING OF THE COLDEST KNOWN BROWN DWARF WITH THE *SPITZER SPACE TELESCOPE*[1]

T. L. Esplin[2], K. L. Luhman[2,3], M. C. Cushing[4], K. K. Hardegree-Ullman[4], J. L. Trucks[4]. A. J. Burgasser[5], & A. C. Schneider[4]

Draft version September 21, 2016

ABSTRACT

Because WISE J085510.83−071442.5 (hereafter WISE 0855-0714) is the coldest known brown dwarf ($\sim$ 250 K) and one of the Sun's closest neighbors (2.2 pc), it offers a unique opportunity for studying a planet-like atmosphere in an unexplored regime of temperature. To detect and characterize inhomogeneities in its atmosphere (e.g., patchy clouds, hot spots), we have performed time-series photometric monitoring of WISE 0855-0714 at 3.6 and 4.5 μm with the *Spitzer Space Telescope* during two 23 hr periods that were separated by several months. For both bands, we have detected variability with peak-to-peak amplitudes of 4–5% and 3–4% in the first and second epochs, respectively. The light curves are semi-periodic in the first epoch for both bands, but are more irregular in the second epoch. Models of patchy clouds have predicted a large increase in mid-IR variability amplitudes (for a given cloud covering fraction) with the appearance of water ice clouds at $T_{\rm eff}$ <375 K, so if such clouds are responsible for the variability of WISE 0855-0714, then its small amplitudes of variability indicate a very small deviation in cloud coverage between hemispheres. Alternatively, the similarity in mid-IR variability amplitudes between WISE 0855-0714 and somewhat warmer T and Y dwarfs may suggest that they share a common origin for their variability (i.e., not water clouds). In addition to our variability data, we have examined other constraints on the presence of water ice clouds in the atmosphere of WISE 0855-0714, including the recent mid-IR spectrum from Skemer et al. (2016). We find that robust evidence of such clouds is not yet available.

Subject headings: brown dwarfs — infrared: stars — solar neighborhood — stars: low-mass — planets and satellites: atmospheres

1. INTRODUCTION

In multiple temperature regimes for brown dwarfs, condensates are predicted to form clouds, which can significantly influence the emergent spectra and colors (Ackerman & Marley 2001). The spectra of L dwarfs (1300–2200 K; Stephens et al. 2009) are best fit by models that include a thick cloud layer of iron, silicates, and corundum (Saumon & Marley 2008). Those clouds break up non-uniformly and disappear as brown dwarfs grow cooler and enter the T dwarf sequence (500–1300 K; Stephens et al. 2009), as indicated by the near-infrared (IR) colors (Burgasser et al. 2002), photometric and spectral variability (Buenzli et al. 2014; Burgasser et al. 2014; Radigan 2014; Radigan et al. 2014; Wilson et al. 2014; Yang et al. 2016), and surface maps (Crossfield et al. 2014; Karalidi et al. 2016) of objects near the L/T transition. Clouds may appear again below 900 K based on the colors of late T dwarfs, this time in the form of sulfides (Morley et al. 2012). Photometric variability at near-IR wavelengths has been reported in this temperature regime, which has been attributed to clouds (Yang et al. 2016). Among the Y dwarfs (<500 K; Dupuy & Kraus 2013), additional clouds of water and ammonia are predicted to form at <350 K and <200 K, respectively (Burrows et al. 2003; Morley et al. 2014a). When water clouds are present, they are expected to be patchy (Morley et al. 2014a), and hence amenable to detection through variability. The only Y dwarfs with published time-series photometry, WISE J140518.39+553421.3 (hereafter WISE 1405+5534) and WISEP J173835.52+273258.9, do exhibit variability but they are likely too warm to have water ice clouds ($\sim$400 K; Cushing et al. 2016; Leggett et al. 2016).

The most promising brown dwarf for the detection of water clouds is WISE J085510.83–071442.5 (hereafter WISE 0855-0714). It is the coldest known brown dwarf ($\sim$250 K; Luhman 2014), making it the most likely one to harbor water clouds. In addition, it is the fourth closest system to the Sun (2.23±0.04 pc; Luhman 2014; Luhman & Esplin 2016), so it is relatively bright for its low luminosity. As with other Y dwarfs[6], WISE 0855-0714 is much too faint at near-IR wavelengths for accurate photometric monitoring (Beamín et al. 2014; Faherty et al. 2014; Kopytova et al. 2014; Luhman 2014; Wright et al. 2014; Luhman & Esplin 2016; Schneider et al. 2016). Currently, such measurements are only feasible in mid-IR bands with the Infrared Array Camera (IRAC; Fazio et al. 2004) on the *Spitzer Space Telescope* (Werner et al. 2004).

In this paper, we present time-series IRAC photome-

[1] Based on observations made with the *Spitzer Space Telescope*, which is operated by the Jet Propulsion Laboratory, California Institute of Technology under a contract with NASA.

[2] Department of Astronomy and Astrophysics, The Pennsylvania State University, University Park, PA 16802; taran.esplin@psu.edu.
[3] Center for Exoplanets and Habitable Worlds, The Pennsylvania State University, University Park, PA 16802.
[4] The University of Toledo, OH 43606
[5] Center for Astrophysics and Space Science, University of California San Diego, La Jolla, CA 92093

[6] WISE 0855-0714 has not been spectroscopically classified, but it is very likely to be a Y dwarf based on its luminosity.

try of WISE 0855-0714 during two 23 hour periods. We begin by describing the observations and data reduction (Section 2). We use these data to characterize the variability of WISE 0855-0714, which is then compared to the predictions of models that produce variability through either patchy clouds or hot spots (Section 3). We conclude by assessing the evidence of water ice clouds in the atmosphere of WISE 0855-0714 from our variability measurements and previous observations (Section 4).

2. OBSERVATIONS AND DATA REDUCTION

In the post-cryogenic mission of *Spitzer*, IRAC collects data with two operable 256 × 256 arrays. Each array has a plate scale of 1.″2 pixel^{-1} and a field of view of 5.′2×5.′2. The arrays simultaneously image adjacent areas of sky in filters centered at 3.6 and 4.5 μm, which are denoted as [3.6] and [4.5], respectively. Point sources in the images have FWHM=1.″7.

To minimize the errors in our time series IRAC photometry of WISE 0855-0714 due to variations in intra-pixel sensitivity (Reach et al. 2005), the images were taken in the "staring mode" with the following strategy (Krick et al. 2015): 1) for each of the two filters, the target was placed on the "sweet spot" for that array, which is a portion of a pixel near the corner of the array in which the sensitivity as a function of intra-pixel position has been well-characterized and 2) prior to collection of the science data, the target was imaged for 30 min at [4.5] to provide time for the spacecraft pointing to settle. Following those steps, WISE 0855-0714 was observed continuously during two 23 hour periods on 2015 March 10 and 2015 August 3. During each period, we obtained 405 images with exposure times of 96.8 s at [4.5], which were immediately followed by 405 images with exposures times of 93.6 s at [3.6]. These data were collected through Astronomical Observation Requests 52667904, 52668160, 52668672, and 52668928 within program 11056 (K. Luhman).

We began our reduction of the data using the Corrected Basic Calibrated Data frames produced by the pipeline at the *Spitzer* Science Center (SSC). We measured positions and fluxes of WISE 0855-0714 in each of those frames with a point response function (PRF) fitting routine in the SSC's Astronomical Point source EXtractor (APEX; Makovoz & Marleau 2005), which produces more accurate IRAC astrometry than other commonly used algorithms (Esplin & Luhman 2016). APEX was used with the default parameters except for a 5×5 pixel fitting region. Because aperture photometry has been measured for most previous time-series data from IRAC, we also applied that method to our data for comparison to the results of PRF fitting. The aperture photometry was measured with `phot` in IRAF using an aperture radius of 1.5 pixels and a background annulus of 3 pixels, which was found to produce the least scatter in photometry for WISE 0855-0714 relative to other annuli. To compare the data from PRF fitting and aperture photometry in a given band, we calculated the median absolute deviation (MAD) of the data and rejected outliers that deviated by $> 3\times$MAD. We then fit the unrejected data using a Nadaraya-Watson regression estimator as implemented in the function `npregbw` from the *np* package (Hayfield & Racine 2008) within R (R Core Team 2013). After dividing the data by that fit to remove intrinsic variability, we recomputed the MAD. The MADs from APEX and `phot` were similar for [4.5], but APEX produced significantly lower values at [3.6], where WISE 0855-0714 is much fainter.

We have investigated methods of correcting for systematic noise in our photometry due to the varying intra-pixel sensitivities. The SSC has measured high-resolution gain maps of the sweet spots for [3.6] and [4.5], which can be used for such corrections. However, because WISE 0855-0714 is much fainter at [3.6] than [4.5], the uncertainties in its positions in individual frames are larger than the sweet spot of [3.6] and thus a correction for varying intra-pixel sensitivities was not possible in that band. At [4.5], the positions of WISE 0855-0714 drifted out of the sweet spot for roughly half of the first epoch, but they remained within it throughout the second epoch. As a result, the latter data were suitable for correction using the SSC's gain map. Applying that correction required that we reduce those data a second time following the SSC's recommended procedure, which is performed with the IDL routines `box_centroider`, `aper`, and `pixel_phase_correct_gauss` (Krick et al. 2015). The application of the gain map predicted a maximum change of $< 0.5\%$ and did not produce a lower MAD or any noticeable change to the intrinsic variability compared to the uncorrected photometry from APEX. We tested an alternative method of correcting for the varying intra-pixel sensitivity from Knutson et al. (2008) and Heinze et al. (2013), but it also did not reduce the MADs for either of the two epochs at [4.5] or alter the variability behavior. Therefore, we have adopted the uncorrected photometry produced by PRF fitting with APEX for both bands and epochs. Typical signal to noise ratios (S/N) for the those data are 10.2/146.8 and 10.9/142.3 for [3.6]/[4.5] in the first and second epochs, respectively. The APEX data are listed in Tables 1 and 2 and are plotted as a function of time in Figure 1. We have omitted from Figure 1 measurements that deviated by more than 3×MAD from the Nadaraya-Watson regression that we calculated previously.

Because IRAC is capable of measuring astrometry with high precision (Esplin & Luhman 2016), it might seem possible to search for perturbations in the astrometry of WISE 0855-0714 due to an unseen companion. However, for any plausible combination of orbital separation and mass ratio, the astrometric perturbations would be too small to detect during a 12-hour period given the the typical astrometric errors of 7 mas for WISE 0855-0714 in individual [4.5] frames and additional systematic errors among those frames.

3. ANALYSIS

3.1. *Variability Characteristics*

As shown in Figure 1, WISE 0855-0714 exhibits noticeable variability in both bands and epochs. For instance, the peak-to-peak amplitudes are 4–5% at both [3.6] and [4.5] in the first epoch. While the light curve of the first epoch appears semi-periodic in both bands, the shape does not follow a single-period sinusoid, which suggests that the mechanism producing the variability evolves on the timescale of hours or is spatially complex (i.e., several spots). The second epoch also shows variability in both filters but is less sinusoidal and has a lower amplitude (3–

4%). The differences between the two epochs indicate that the light curve evolves on a timescale of months. These IRAC data have provided the third detection of variability in a (likely) Y dwarf (Cushing et al. 2016; Leggett et al. 2016). The light curves for WISE 0855-0714 are roughly similar to those of the previously studied Y dwarfs in terms of amplitudes, but they are less periodic. In addition to our two epochs of time-series photometry, WISE 0855-0714 has been briefly imaged with *Spitzer* on several other occasions across a period of two years (Luhman 2014; Melso et al. 2015; Luhman & Esplin 2016). Among all of the available photometry, the [3.6] and [4.5] data have spanned ranges of ∼0.16 and 0.13 mag, respectively.

Our attempts to identify a single rotational period for WISE 0855-0714 have produced inconclusive results. The peaks in power in Lomb-Scargle periodograms (Lomb 1976; Scargle 1982) appear at 6.8/9.3 and 9.0/5.3 hrs for [3.6]/[4.5] at the first and second epochs, respectively. We also fit the data in each band and epoch to a double sine model where the second sine has a period twice that of the first (Cushing et al. 2016). While this model produces random residuals, indicating a good fit, the predicted periods are only consistent between epochs at the two sigma level. Specifically, they have values of $9.7^{+0.9}_{-0.8}/10.8^{+0.7}_{-0.7}$ and $14^{+2}_{-2}/13.3^{+0.5}_{-0.4}$ hrs for [3.6]/[4.5] in the first and second epochs, respectively. Mancini et al. (2015) successfully estimated a rotation period for a brown dwarf with a rapidly changing light curve with a more complicated model, but that model fails to converge on a solution for WISE 0855-0714. Additional time-series data would be needed to reliably measure the rotation period and the relative phase between the light curves of the two bands.

Because the spectra of cold brown dwarfs are non-Planckian, different wavelengths can sample different pressure levels in the atmosphere. In the case of WISE 0855-0714, the similarity between the [3.6] and [4.5] light curves at both epochs indicate that they may be sampling similar levels. However, without a measurement of a relative phase between the light curves of the two bands, it is difficult to make strong predictions about the structure of the atmosphere of WISE 0855-0714. For example, an absence of a phase offset between bands would indicate that dynamical circulation is efficiently carrying thermal energy through these pressure levels.

Photometric variability in brown dwarfs could potentially arise from a number of spot-producing mechanisms, including magnetic activity, atmospheric chemical abundance variations, non-uniform cloud coverage, and variable temperature profiles causing hot/cold spots. In the following two sections, we discuss whether the variability of WISE 0855-0714 can be explained by the latter two mechanisms. We have not considered the first two mechanisms because light curves have not been modeled for an atmosphere with heterogenous chemical abundances and because magnetically-induced starspots probably do not form in the neutral atmospheres of the coldest brown dwarfs, even in the presence of magnetic fields (e.g., Mohanty et al. 2002).

3.2. *Patchy Water Clouds*

If water clouds are present in the atmospheres of brown dwarfs as cold as WISE 0855-0714, those clouds are likely to be patchy rather than uniform (Morley et al. 2014a). To construct a self-consistent and stable model with non-uniform cloud coverage, Morley et al. (2014a) computed emergent spectra for cloudy and clear atmospheric columns with a single temperature-pressure profile and then combined the fluxes (F_ν) from the two columns in the following manner:

$$F_{\nu,\mathrm{total}} = hF_{\nu,\mathrm{clear}} + (1-h)F_{\nu,\mathrm{cloudy}}, \quad (1)$$

where h is the fraction of the atmosphere without clouds (Marley et al. 2010). Any deviation of h between hemispheres from the global average of a model for WISE 0855-0714 would produce photometric variability. In addition, these patchy cloud models predict substantially different emergent flux between the clear and cloudy columns at the two IRAC bands. For example, in Figure 2 we show the spectra of both columns for a model brown dwarf with T_{eff}=250 K, log g=4.0 cm s^{-2}, f_{sed}[7]=3 and a cloud coverage of 50% (h= 0.5) (Morley et al. 2014a)[8]. The cloudy column exhibits much lower flux longward of ∼3 μm while the near-IR spectrum is affected less by the presence of water clouds. As a result, our IRAC observations are ideal for detecting photometric variability produced from water clouds.

To test whether water clouds can produce the observed variability in WISE 0855-0714, we follow the prescription of Cushing et al. (2006, 2016). Using the h=0.5 model of Figure 2, we assumed that the cloud cover between hemispheres deviates from the global average by Δh and calculated predicted fluxes for $F_{\nu,h+\Delta h}$ and $F_{\nu,h-\Delta h}$ from Equation 1. This deviation would produce variability with a semi-amplitude of

$$A_\lambda = \frac{\max\left[\mathrm{F}_{\nu,\mathrm{h}+\Delta\mathrm{h}}(\lambda), \mathrm{F}_{\nu,\mathrm{h}-\Delta\mathrm{h}}(\lambda)\right]}{\mathrm{average}\left[\mathrm{F}_{\nu,\mathrm{h}+\Delta\mathrm{h}}(\lambda), \mathrm{F}_{\nu,\mathrm{h}-\Delta\mathrm{h}}(\lambda)\right]} - 1. \quad (2)$$

In Figure 3, we show the predicted semi-amplitudes at [3.6] and [4.5] as a function of Δh for T_{eff}=250 K, log g=4.0 cm s^{-2}, cloud coverage of 50%, and f_{sed}=3, 5 and 7. Amplitudes in the two bands do not differ significantly for $\Delta h < 0.05$ and increase linearly with increasing deviation from homogeneous cloud cover. We find that only a small deviation from a global average h ($\Delta h \approx 0.01$) is needed to reproduce the observed amplitudes of variation in both bands for WISE 0855-0714. Although this model of patchy clouds is able to reproduce the observed variability of WISE 0855-0714, it may not be the best explanation of those data, as discussed in Section 4.

3.3. *Hot Spots*

A brown dwarf's photometric variability could be produced by temperature perturbations in its atmosphere, which would be manifested as time-varying hot and/or cold spots in the photosphere. Such perturbations might occur if the atmosphere circulates faster than the gas can

[7] This parameter describes the efficiency of cloud particle growth, or sedimentation (Ackerman & Marley 2001), where higher values correspond to larger particle sizes and consequently geometrically thinner clouds.

[8] The combined spectra from the cloudy and clear columns in the models from Morley et al. (2014a) are available at www.ucolick.org/∼cmorley/cmorley/Models.html. We have made use of the separate spectra from those columns, which were provided by C. Morley.

equilibrate or if the photosphere is radiatively coupled to changes at deeper pressure levels, such as deep heterogeneous clouds (Showman & Kaspi 2013; Robinson & Marley 2014). Morley et al. (2014b) simulated the effect of the latter mechanism by injecting energy at various pressure levels into cloudless static models for brown dwarfs with temperatures of 400–1000 K. Cushing et al. (2016) performed the same exercise for 500 K in an attempt to reproduce the variability of WISE 1405+5534. The two studies found that spots produce large variability in strong absorption features like the CH_4 band within the [3.6] band, whereas the variability was smaller at wavelengths with less absorption, as in the case of [4.5]. In contrast, WISE 0855-0714 exhibits similar variability amplitudes in those two bands. Thus, it appears unlikely that hot spots are the cause of its variability.

4. DISCUSSION

Previous studies have attempted to constrain the presence of water ice clouds in the atmosphere of WISE 0855-0714 using photometry and spectroscopy. Faherty et al. (2014) reported a possible 2.6 σ detection of WISE 0855-0714 in a medium-band filter within the J band. Those data were used to place the object in a diagram of M_{W2} versus $J - W2$, where $W2$ is a band from the *Wide-field Infrared Survey Explorer* (Wright et al. 2010) that is similar to [4.5] from *Spitzer*. The position of WISE 0855-0714 in that diagram was better reproduced by cloudy models than cloudless models (Morley et al. 2012, 2014a; Saumon et al. 2012), which was interpreted as evidence of water ice clouds. However, Luhman & Esplin (2014) demonstrated that WISE 0855-0714 was roughly midway between those cloudless and cloudy models in a similar diagram of $M_{4.5}$ versus $J-[4.5]$, and that its position was best matched by cloudless models that employed non-equilibrium chemistry (Saumon & Marley 2008; Saumon et al. 2012). After measuring photometry for WISE 0855-0714 in several additional near-IR bands, Schneider et al. (2016) and Luhman & Esplin (2016) found that no single suite of models provided a clearly superior match to the observed spectral energy distribution (SED), and that all of the models differed significantly from the data. Thus, the photometry and models that are currently available do not provide any indication of whether water ice clouds are present in WISE 0855-0714.

A spectroscopic investigation of water ice clouds in WISE 0855-0714 has been recently performed by Skemer et al. (2016). They obtained the only spectrum to date of the brown dwarf, which spans from 4.5–5.1 μm. Although its resolution and S/N were low, the spectrum exhibited absorption features that appeared to be statistically significant, many of which coincided with features in model spectra computed by Skemer et al. (2016). The spectra predicted by cloudless and partly cloudy models were indistinguishable for the wavelength range and resolution of the data. The atmospheric temperature structure for a brown dwarf near the temperature of WISE 0855-0714 does not converge with full coverage of water clouds (Morley et al. 2014a), so Skemer et al. (2016) developed a simplified model for that scenario, which used a gray, fully absorbing cloud with no specified composition. The cloud-top pressure in that model was varied to optimize the match to the observed spectrum. The resulting best-fit spectrum agreed somewhat better with the data than the spectra from the cloudless and partly cloudy models, which was cited as a detection of clouds. Given the temperature of WISE 0855-0714, it is expected that such clouds would be composed of water (Burrows et al. 2003; Morley et al. 2014a).

It is unclear whether the spectrum from Skemer et al. (2016) actually contains evidence of water clouds. The fully cloudy model from that study considered gray absorbers, whereas water ice is non-gray across the wavelength range of the spectrum of WISE 0855-0714 (Morley et al. 2014a), and it assumed that the cloud coverage is uniform, which is not expected for water clouds (Morley et al. 2014a). In addition, models with patchy clouds have self-consistent temperature structures, which has not been possible for the fully cloudy models (Morley et al. 2014a). Given the variety of uncertainties in models of the coldest brown dwarfs (Morley et al. 2014a) and the large differences between the observed and predicted SEDs for WISE 0855-0714 (Schneider et al. 2016; Luhman & Esplin 2016), the current models may not be sufficiently accurate for subtle differences in predicted spectra to provide meaningful insight into the physical properties of WISE 0855-0714.

Our variability measurements can provide additional constraints on the existence of water ice clouds in the atmosphere of WISE 0855-0714. According to the partly cloudy models of Morley et al. (2014b), cloud-induced variability at mid-IR wavelengths should become much larger (for a given cloud covering fraction) at temperatures below $\sim$ 375 K with the onset of water clouds. The amplitudes that we have measured for WISE 0855-0714 ($\sim$ 250 K) are only a few percent, which would require very small deviations in cloud coverage between hemispheres ($\Delta h \sim 0.01$) if water clouds are responsible for the variability. Meanwhile, the mid-IR amplitudes for WISE 0855-0714 are similar to those observed for early Y dwarfs ($\sim$ 400 K, Cushing et al. 2016; Leggett et al. 2016) and late T dwarfs (800–1000 K, Metchev et al. 2015; Yang et al. 2016), which should be too warm to harbor water clouds. If water clouds are producing the variability of WISE 0855-0714, then it must coincidentally have a value of Δh that produces roughly the same amplitudes as the different variability mechanism that operates in those objects. Alternatively, the similarity in the amplitudes of WISE 0855-0714 and somewhat warmer brown dwarfs may indicate that they share a common origin for their variability (i.e., not water clouds). Based on these results and the previous work that we have discussed, we conclude that robust evidence of water clouds in the atmosphere of WISE 0855-0714 is not yet available.

We thank Caroline Morley and Mark Marley for providing their model calculations. We acknowledge support from a grant from NASA issued by the Jet Propulsion Laboratory (JPL), California Institute of Technology. The *Spitzer Space Telescope* is operated by JPL/Caltech under a contract with NASA. The Center for Exoplanets and Habitable Worlds is supported by the Pennsylvania State University, the Eberly College of Science, and the Pennsylvania Space Grant Consortium.

REFERENCES

Ackerman, A. S., & Marley, M. S. 2001, ApJ, 556, 872
Beamín, J. C., Ivanov, V. D., Bayo, A., et al. 2014, A&A, 570, L8
Buenzli, E., Apai, D., Radigan, J., Neill, R. I., & Davin, F. 2014, ApJ, 782, 77
Burgasser, A. J., Gillon, M., Faherty, J., et al. 2014, ApJ, 785, 48
Burgasser, A. J., Marley, M. S., Ackerman, A. S., et al. 2002, ApJ, 571, L151
Burrows, A., Sudarsky, D., & Hubbard, W. B. 2003, ApJ, 594, 545
Crossfield, I. J. M., Biller, B., Schlieder, J. E., et al. 2014, Nature, 505, 654
Cushing, M. C., Hardegree-Ullman, K. K., Trucks, J. L., et al. 2016, ApJ, 823, 152
Cushing, M. C., Roellig, T. L., Marley, M. S., et al. 2006, ApJ, 648, 614
Dupuy, T. J. & Kraus, A. L. 2013, Sci, 341, 1492
Esplin, T. L. & Luhman, K. L. 2016, AJ, 151, 9
Faherty, J. K., Tinney, C. G., Skemer, A., & Monson, A. J. 2014, ApJ, 793, L16
Fazio, G. G., Hora, J. L., Allen, L. E., et al. 2004, ApJS, 154, 10
Hayfield, T. & Racine, J. S. 2008, Journal of Statistical Software, 27, 5
Heinze, A. N., Metchev, S. A., Apai, D., et al. 2013, ApJ, 767, 173
Karalidi, T., Apai, D., Marley, M. S., & Buenzli, E. 2016, ApJ, 825, 90
Krick, J., Ingalls, J., Carey, S., et al. 2015, IRAC High Precision Photometry Website, `http://irachpp.spitzer.caltech.edu`
Kopytova, T. G., Crossfield, I. J., Deacon, N. R., et al. 2014, ApJ, 797, 3
Knutson, H. A., Charbonneau, D., Allen, L. E., Burrows, A., & Megeath, S. T. 2008, ApJ, 673, 526
Leggett, S. K., Cushing, M. C., Kardegree-Ullman, K. K., et al. 2016, ApJ, in press
Lomb, N. R. 1976, Ap&SS, 39, 447
Luhman, K. L. 2014, ApJ, 786, L18
Luhman, K. L. & Esplin, T. L. 2014, ApJ, 796, 6
Luhman, K. L. & Esplin, T. L. 2016, AJ, 152, 78
Makovoz, D., & Marleau, F. R. 2005, PASP, 117, 1113
Mancini, L., Giacobbe, P., Littlefair, S. P., et al. 2015, A&A, 584,104
Marley, M. S., Saumon, D., & Goldblatt, C. 2010, ApJ, 723, L117
Melso, N. D., Kaldon, K. M., & Luhman, K. L. 2015, AJ, 150, 62
Metchev, S. A., Heinze, A., Apai, D., et al. 2015, ApJ, 799, 154
Mohanty, S., Basri, G., Shu, F., Allard, F., & Chabrier, G. 2002, ApJ, 571, 469
Morley, C. V., Fortney, J. J., Marley, M. S., et al. 2012, ApJ, 756, 172
Morley, C. V., Marley, M. S., Fortney, J. J., & Lupu, R. 2014b, ApJ, 789, L14
Morley, C. V., Marley, M. S., Fortney, J. J., et al. 2014a, ApJ, 787, 78
R Core Team 2013, R Foundation for Statistical Computing, Vienna, Austria, www.R-project.org
Radigan, J. 2014, ApJ, 797, 120
Radigan, J., Lafreniére, D., & Jayawardhana, R. 2014, ApJ, 793, 75
Reach, W. T., Megeath, S. T., Cohen, M., et al. 2005, PASP, 117, 978
Robinson, T. D., & Marley, M. S. 2014, ApJ, 785, 158
Saumon, D., & Marley, M. S. 2008, ApJ, 689, 1327
Saumon, D., Marley, M. S., Abel, M., Frommhold, L., & Freedman, R. S. 2012, ApJ, 750, 74
Scargle, J. D. 1982, ApJ, 263, 835
Schneider, A. C., Cushing, M. C., Kirkpatrick, J. D., & Gelino, C. R. 2016, ApJ, 823, L35
Showman, A. P., & Kaspi, Y. 2013, ApJ, 776, 85
Skemer, A. J., Morley, C. V., Allers, K. N., et al. ApJ, 826, L17
Stephens, D. C., Leggett, S. K., Cushing, M. C., et al. 2009, ApJ, 702, 154
Werner, M. W., Roellig, T. L., Low, F. J., et al. 2004, ApJS, 154, 1
Wilson, P. A., Rajan, A., & Patience, J. 2014, A&A, 566, 111
Wright, E. L., Mainzer, A., Kirkpatrick, J. D., et al. 2014, AJ, 148, 82
Wright, E. L., Eisenhardt, P. R. M., Mainzer, A. K., et al. 2010, AJ, 140, 1868
Yang, H., Apai, D., Marley, M. S., et al. 2016, ApJ, 826, 8

TABLE 1
Time-series Photometry for
WISE 0855-0714 in [3.6]

HMJD	[3.6] (mag)	error (mag)	Outlier?
57091.0253	17.669	0.099	Y
57091.0264	17.282	0.066	N
57091.0276	17.258	0.064	N
57091.0288	17.380	0.071	N
57091.0300	17.411	0.073	N

Note. — Photometry is absent for four frames because APEX failed to converge on a measurement. This table is available in its entirety in a machine-readable format. A portion is shown here for guidance regarding its form and content.

TABLE 2
Time-series Photometry for
WISE 0855-0714 in [4.5]

HMJD	[4.5] (mag)	error (mag)	Outlier?
57090.5488	13.876	0.008	Y
57090.5500	13.840	0.007	N
57090.5512	13.854	0.007	N
57090.5523	13.846	0.007	N
57090.5535	13.855	0.007	N

Note. — Photometry is absent for one frame because APEX failed to converge on a measurement. This table is available in its entirety in a machine-readable format. A portion is shown here for guidance regarding its form and content.

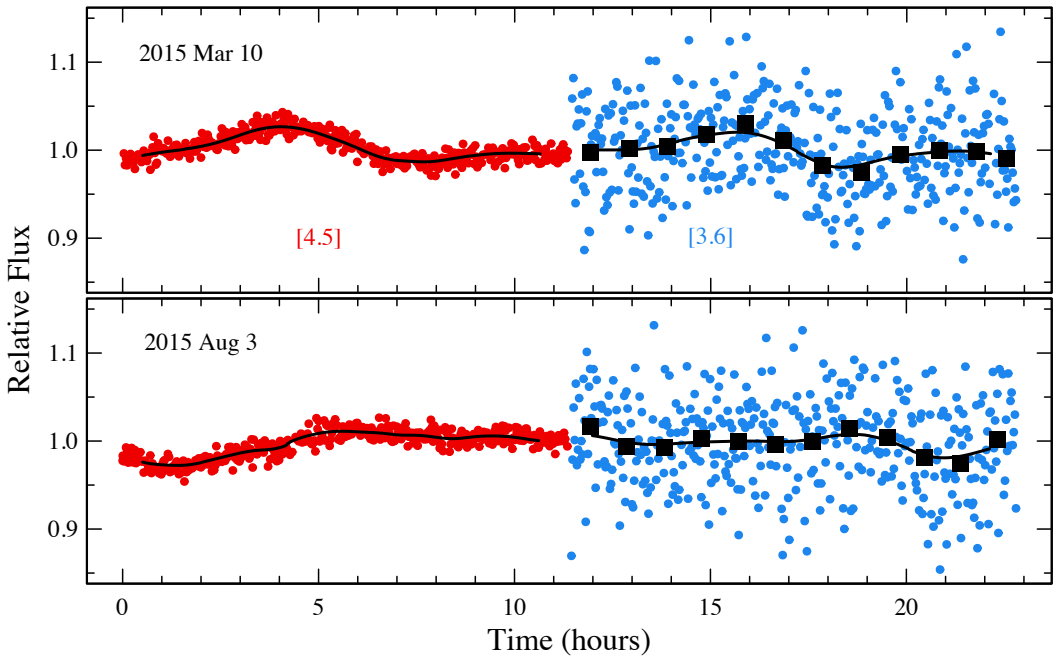

FIG. 1.— Time-series IRAC photometry of WISE 0855-0714 during two 23 hour periods. To illustrate the variability in these data, we include a **non-parametric** fit to the light curve for each band and epoch (black lines) and we have binned the [3.6] data into 12 equal time intervals (solid squares). Measurements that differed from the fits by >3×MAD have been omitted.

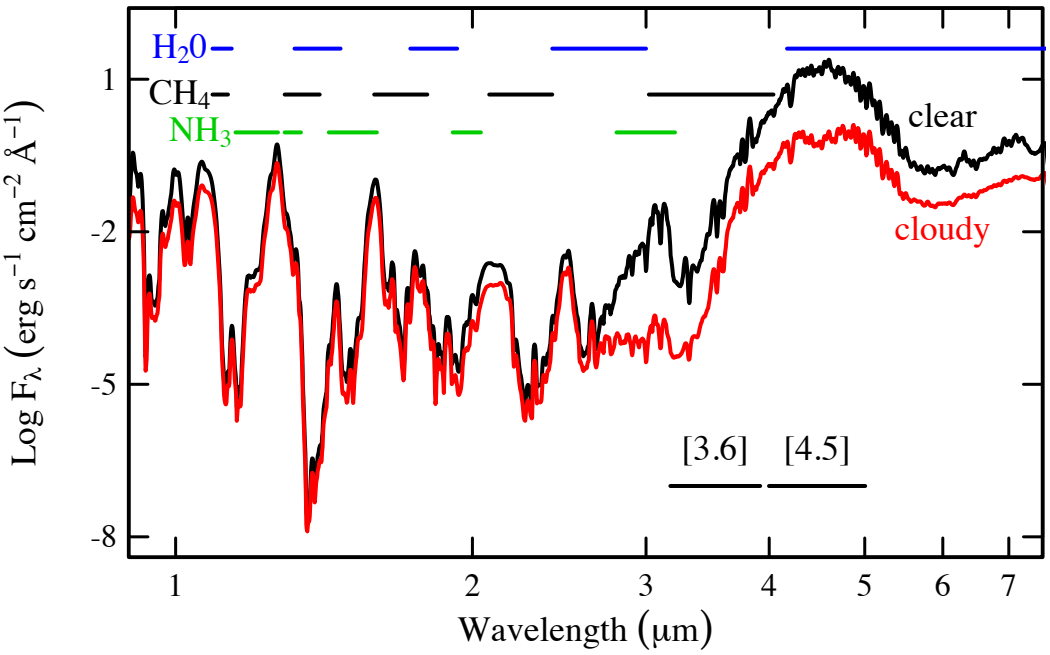

FIG. 2.— Model spectra for clear (black) and cloudy (red) columns in the atmosphere of a brown dwarf with $T_{\rm eff}$=250 K, log g=4.0 cm s^{-2}, $f_{\rm sed}$=3, and a cloud coverage of 50% (h = 0.5; Morley et al. 2014a). The wavelengths of prominent molecular absorption bands and the [3.6] and [4.5] filters are indicated. Longward of ∼3 μm, water clouds are predicted to significantly reduce the emergent flux. Any deviation of the cloud coverage fraction between hemispheres would produce rotationally-modulated variability at [3.6] and [4.5].

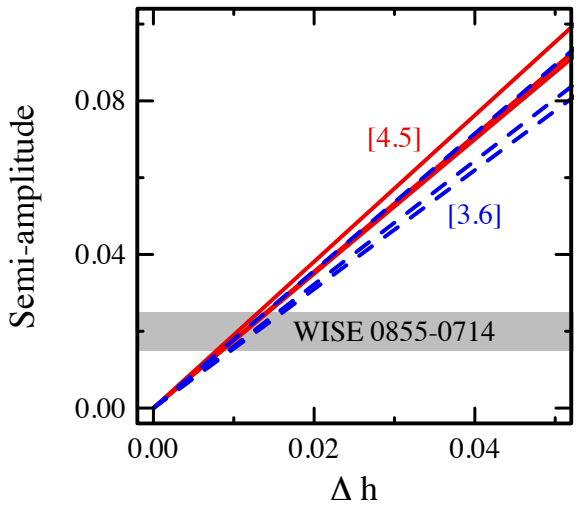

FIG. 3.— Predicted semi-amplitudes of variability for [3.6] (blue) and [4.5] (red) assuming a deviation in the cloud coverage fraction of Δh from a global average (h=0.5) between hemispheres for the model from Figure 2 (Morley et al. 2014a) **with $f_{\rm sed}$=3, 5, and 7, which correspond to the middle, top, and bottom lines for each band, respectively.** The observed semi-amplitudes for the two bands are similar for WISE 0855-0714 (gray region). Only a 1% deviation in the cloud coverage is needed to explain the observations.